Advancing Atmospheric Thermodynamic Sounding From Space Using Hyperspectral Microwave Measurements

Antonia Gambacorta, Jeffrey Piepmeier, *Fellow, IEEE*, Mark Stephen, Joseph Santanello, John Blaisdell, Isaac Moradi, William McCarty, Robert Rosenberg, Alexander Kotsakis, Fabrizio Gambini, Priscilla Mohammed, *Member, IEEE*, Rachael Kroodsma, *Member, IEEE*, James MacKinnon, Ian Adams, and Paul Racette

***Abstract*—In this article, we present a comprehensive sensitivity analysis and geophysical retrieval product demonstration to assess the enhanced information content in atmospheric temperature and water vapor, harnessed in hyperspectral microwave measurements. A particular focus of this study is devoted to quantifying and comparing the impact on retrieval performance resulting from novel spectral bands of the microwave thermal spectrum, by means of data addition and data denial trade studies. Various spectral configurations are assessed, each reflecting specific technology solutions intended to maximize geophysical product performance within feasible size, weight, power, and cost constraints. Our results indicate that the use of a hyperspectral sampling in the oxygen and water vapor sounding lines alone provides significant improvements in the lower and free tropospheric thermodynamic fields (up to ∼40%), when compared against the program of record (i.e., the Advanced Technology Microwave Sounder, ATMS). Our experiments also demonstrate the essential role played by extending the coverage in the window regions, leading to an overall improvement of up to ∼50% in the Earth's planetary boundary layer thermodynamic fields. This work concludes with an overview on the state of the art in hyperspectral microwave technology and a discussion on future applications of interest to numerical weather prediction and climate science. The work presented in this study focuses on ocean, clear-sky demonstrations. All-sky, all-surface investigations will be the focus of a follow-up study, as we advance our capability to simulate more complex scenarios and improve scene variability.**

***Index Terms*—Hyperspectral, microwave, observations simulations sensitivity experiments, PICASIC, photonic integrated circuits, planetary boundary layer (PBL), satellite remote sensing.**

Manuscript received 28 February 2022; revised 29 October 2022 and 23 March 2023; accepted 8 April 2023. Date of publication 25 April 2023; date of current version 14 June 2023. This work was supported by NASA's Earth Science Technology Office (ESTO) through the NRA NNH19ZDA001N, Instrument Incubator Program (IIP). *(Corresponding author: Antonia Gambacorta.)*

Antonia Gambacorta, Jeffrey Piepmeier, Mark Stephen, Joseph Santanello, James MacKinnon, Ian Adams, and Paul Racette are with the NASA Goddard Space Flight Center, Greenbelt, MD 20771 USA (e-mail: antonia.gambacorta@nasa.gov; jeffrey.r.piepmeier@nasa.gov; mark.a.stephen@nasa.gov; Joseph.A.Santanello@nasa.gov; james.mackinnon@nasa.gov; ian.s.adams@nasa.gov; paul.e.racette@nasa.gov).

John Blaisdell and Robert Rosenberg are with the Science Applications International Corporation, Reston, VA 12010 USA, and also with the NASA Goddard Space Flight Center, Greenbelt, MD 20771 USA (e-mail: John.Blaisdell@nasa.gov; robert.i.rosenberg@nasa.gov).

Isaac Moradi and Rachael Kroodsma are with the Earth System Science Interdisciplinary Center, University of Maryland, College Park, MD 20742 USA, and also with the NASA Goddard Space Flight Center, Greenbelt, MD 20771 USA (e-mail: isaac.moradi@nasa.gov; rachael.a.kroodsma@nasa.gov).

William McCarty is with the NASA Headquarter, Washington, DC 39529 USA (e-mail: will.mccarty@nasa.gov).

Fabrizio Gambini is with the Center for Space Sciences and Technology, University of Maryland, Baltimore County, MD 20742 USA, and also with the Center for Research and Exploration in Space Science and Technology, NASA Goddard Space Flight Center, Greenbelt, MD 20771 USA (e-mail: fabrizio.gambini@nasa.gov).

Priscilla Mohammed is with the Morgan State University, NASA Goddard Space Flight Center, Greenbelt, MD 20771 USA (e-mail: Priscilla.N.Mohammed@nasa.gov).

Alexander Kotsakis is with the ERT, Inc., Laurel, MD 20771 USA, and also with the NASA Goddard Space Flight Center, Greenbelt, MD 20771 USA (e-mail: alexander.e.kotsakis@nasa.gov).

Digital Object Identifier 10.1109/JSTARS.2023.3269697

I. Introduction

HYPERSPECTRAL (a few hundred to a few thousand channels) microwave sensors have been strongly advocated by space and meteorological agencies worldwide, to augment the Earth's atmospheric sounding capability of temperature and water vapor from space [1], [2], [3], [4], [5]. The National Aeronautics and Space Administration (NASA) Planetary Boundary Layer (PBL) Incubation Study Team Report highlighted hyperspectral microwave sensors as an *essential component* to fly in a potential future PBL observing system [6]. In a recent Broad Agency Announcement, the National Oceanic and Atmospheric Administration requested recommendations for a hyperspectral microwave sensor (HyMS) technology concept and a demonstration of its effectiveness to advance operational numerical weather prediction (NWP) from space.

Existing microwave sensors have demonstrated a large applicability in NWP and climate applications, thanks to their capability to measure all three phases of water and their sensitivity to all forms of precipitation ([9], [10], [11], [12], [13], [14], [15] to cite a few). While liquid droplets and ice particles make most clouds opaque in the infrared, the microwave is still partially transparent [8], [22]. This enables sounding of vertical temperature and water vapor under all-sky conditions. Operational passive microwave space-borne sensors from the current program of record (e.g., the advanced atmospheric microwave sounder, ATMS, [16]), the time-resolved observations of precipitation structure and storm intensity with a constellation of smallsats (TROPICS, [17]) and even planned sensors (e.g., the microwave

© 2023 The Authors. This work is licensed under a Creative Commons Attribution-NonCommercial-NoDerivatives 4.0 License. For more information, see https://creativecommons.org/licenses/by-nc-nd/4.0/

sounder, the micro wave imager, and ice cloud imager (ICI) [18], [19]), however, have only a couple dozen channels, sparsely sampled across the thermal microwave spectrum. This constrains the information content in the measurement to only a few degrees of freedom, limiting vertical resolution and accuracy in the retrieved thermodynamic fields. The Earth's PBL is the most affected region, due to the strong attenuation introduced by the overlying absorbing gas layers in the free troposphere.

The reason for stalled progress in hyperspectral microwave technology rests in the numerous technological challenges associated with simultaneously processing an ultrawide bandwidth, at hyperspectral resolution (<1 GHz), while maintaining a feasible instrument size, weight, and power consumption, and cost (SWaP-C). Recent advances in sensor component technology, however, have allowed the hyperspectral sampling of the microwave region to become a more realistic and cost-effective possibility. To that end, assessing the information content that can be gained from the various bands of the thermal microwave spectrum is important toward informing the engineering design and the technology decisions that will ultimately lead to the next generation of hyperspectral microwave sensors from space.

Pioneering studies ([1], [2], [3], [4], [5], [21], [22], [23], [24]) have conducted simulation experiments on the use of increased spectral coverage (i.e., the 63–67 GHz, 118 GHz bands and novel window channels) and improved resolution in the conventional spectral bands (i.e., the 50–57 GHz and 183 GHz bands). The overarching conclusion of these studies was that hyperspectral microwave sounding can significantly increase information content and thermodynamic sounding capabilities, under both clear and cloudy sky scenarios. In this work, we extend these analyses by performing an end-to-end temperature and water vapor retrieval statistical analysis, comparing multiple spectral configurations. We are particularly interested in quantifying and comparing the impact on the retrieval performance resulting from the use of different bands and channels, by means of data addition and data denial trade studies. In doing so, we assess different spectral configurations, each reflecting specific engineering design and technology solutions intended to obtain improved geophysical product performance within feasible SWaP-C.

Section II provides a spectral sensitivity study to atmospheric temperature and water vapor across the 6–250-GHz spectral domain. This analysis serves the purpose of assessing and comparing sensitivity characteristics across the spectrum and provides a critical role in informing observation simulation sensitivity experiments (OSSE) configurations and geophysical retrieval product performance. As in [4] and [5], we plan to parse our OSSEs into two steps, focusing this study on an end-to-end temperature and water vapor clear-sky study first. All-sky hydrometeors, temperature and water vapor OSSEs are underway, as we advance our capability to simulate more complex scenes and improve scene variability. Results of this second phase of experiments will be the subject of a follow up publication. We then assess retrieval vertical resolution and sensitivity gained from the use of a more extended coverage and higher resolution in the microwave thermal spectrum. Finally, we assess the impact on retrieval performance by analyzing a global, clear-sky ensemble of retrieval results and compare multiple configurations to inform future decisions on engineering design. This work concludes with an overview on the state of art in hyperspectral microwave technology and provides few directions for future applications beneficial to NWP and climate science.

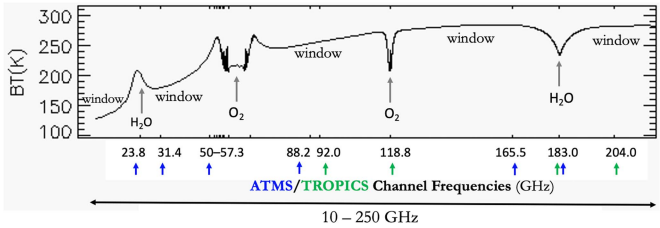

Fig. 1. Illustration of a simulated brightness temperature spectrum over the full, contiguous thermal microwave domain (6–250 GHz), as it would be measured from a space-borne sensor. Oxygen spin-rotation transitions comprise approximately 30 lines between 50 and 70 GHz and an isolated line at 118.75 GHz. Water vapor has a weak rotational line at 22.23 GHz that is semitransparent at normal atmospheric humidity, and a much stronger, opaque line at 183.31 GHz. At frequencies away from these two lines, microwave absorption by water vapor is predominantly from the continuum, which is attributed to the low-frequency wing of the intense infrared and submillimeter rotational band lines. Blue and green arrows locate the ATMS and TROPICS frequencies across the spectrum. The simulation has been performed using the community radiative transfer model (CRTM, [26]) using a mid-latitude, ocean, atmospheric truth.

II. Observation Simulation Sensitivity Experiments

A. Spectral Sensitivity Study

In the thermal microwave domain, the most active atmospheric molecules are oxygen and water vapor. The oxygen molecule has only a magnetic dipole moment, and the associated rotational transition lines are intrinsically much weaker than those resulting from the electric dipole vibrational transitions of the water vapor molecule. However, oxygen has a much higher abundance in the atmosphere and this feature provides adequate signal to be measured from a space borne sensor. When clouds are present, liquid water also plays a role in the radiative transfer process. However, common water and ice clouds particles are small compared to the microwave wavelength, hence generally more transparent when compared to the infrared domain. Fig. 1 illustrates the simulation of a brightness temperature spectrum across the full, contiguous thermal microwave domain (6–250 GHz) as it would be measured from a space-borne hyperspectral microwave sensor over a mid-latitude, ocean surface. Oxygen spin-rotation transitions comprise approximately 30 lines between 50 and 70 GHz and an isolated line at 118.75 GHz. Water vapor has a weak rotational line at 22.23 GHz that is semitransparent at normal atmospheric humidity, and a much stronger, opaque line at 183.31 GHz. At frequencies away from these two lines, microwave absorption by water vapor is predominantly from the continuum, which is attributed to the low-frequency wings of the intense infrared and submillimeter rotational band lines [20]. Due to their relative transparency to the atmospheric gases, these interstitial bands are commonly referred to as *window* bands, as they act like windows through which a space-borne sensor can *see* the surface emitted signal.

TABLE I
SPECTRAL AND NOISE CHARACTERISTICS OF THE HYPERSPECTRAL MICROWAVE CONFIGURATION USED IN THIS STUDY

Channel Frequency (GHz)	Spectral Resolution (MHz)	Instrument Noise (K)	Number of Channels
52.6–57.3 and 63.3–67.9	10	2.1	940
113.7–123.7	20	1.5	510
173.3–193.3	40	1.0	510
6.92	350	0.3	1
10.65	100	0.7	1
15.37	150	0.5	1
18.70	200	0.5	1
21.3	200	0.5	1
22.35	290	0.4	1
23.80 *	400	0.3	1
31.65 *	300	0.4	1
36.50	1000	0.2	1
40.25	500	0.3	1
50.30 *	200	0.5	1
89.0 *	3000	0.1	1
101.0	2000	0.1	1
110.65	1300	0.2	1
150.00 **	3000	0.1	1
157.00	3000	0.1	1
165.5 *	3000	0.1	1
202.00	3000	0.1	1
207.00	3000	0.1	1
229.00	3000	0.1	1
237.00	3000	0.1	1
251.00	3000	0.1	1

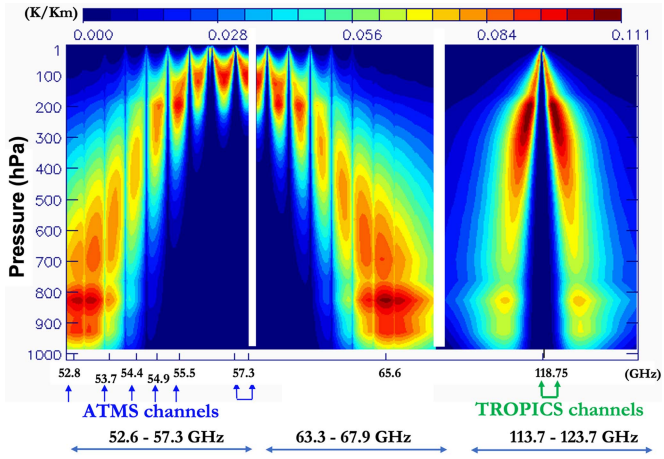

Fig. 2. Temperature Jacobians in the 52.6–57.3 GHz, 63.3–67.9 GHz, and 118 GHz spectral channels listed in Table I. 1-K temperature perturbations in each 1-km-pressure layer of the atmospheric profile have been applied to measure the response in brightness temperature at each frequency in the two bands, using 10 and 20-MHz spectral resolution, respectively. The figure illustrates the rich structure and high sensitivity to temperature harnessed through a contiguous and high resolution spectral coverage of the microwave thermal spectrum, and largely missed from the sparse spectral sampling characterizing the program of record (blue and green arrows indicate the location of ATMS and TROPICS channels, respectively). Of particular interest is the enhanced sensitivity in the Earth's Planetary Boundary Layer, where the highest impact on temperature retrieval performance will be observed (see ahead, retrieval demonstrations).

Hyperspectral coverage in the window region is critical to infer surface properties and is also key to differentiate among different atmospheric hydrometeors (e.g., cloud ice/liquid water, all forms of precipitation), enabling all-sky retrieval capabilities [2].

The hyperspectral microwave configuration used in this study is described in Table I. This configuration resembles that examined in [4] and [5]. The 52.6–57.3-GHz and 63.3–67.9-GHz portions of the oxygen band (altogether defined as the "60 GHz band") are sampled with a spectral resolution of 10 MHz. As in [4] and [5], we acknowledge the redundancy present in the center of this band, predominantly sensitive to the high reaches of the troposphere. Since our interest is in increasing vertical sensitivity along the full vertical column, mindful of SWaP-C constraints, we focus our study on these two lateral portions. The 113.7–123.7-GHz oxygen band ("118-GHz band") is sampled with a spectral resolution of 20 MHz. The 173.3–193.3-GHz water vapor band ("183 GHz band") is sampled with a spectral resolution of 40 MHz. We will study the contribution of novel channels across multiple window regions of the microwave spectrum and assess their impact on improved sensitivity and retrieval performance. These novel channels are also the same, as in [4], and are listed in Table I (rows 4 to 25). Channels marked by one asterisk indicate conventional channels in use on ATMS. Channels marked by double asterisks are advanced microwave sounding unit (AMSU) channels.

The third column in Table I lists the predicted instrument noise performance derived from the classic radiometric formula in (1). The noise equivalent delta temperature (NEdT) value of the receiver (T_{rec}) was estimated using a nominal noise figure of broadband microwave amplifiers. We used an equivalent antenna temperature (T_{ant}) of 270 K and an integration time (τ) as in ATMS (18 ms). The spectral bandwidths $\Delta\nu$ are those listed in Table I

$$\text{NEdT} = (T_{\text{rec}} + T_{\text{ant}})/\sqrt{\Delta\nu * \tau}. \quad (1)$$

For comparison purposes, Table II provides the equivalent channel spectral and noise characteristics for ATMS. Instrument noise values are derived from [25] and represent measured ATMS channel noise values.

Figs. 2–4 provide a comprehensive overview of the measured brightness temperature sensitivity to atmospheric temperature and water vapor across the 6–250-GHz spectral domain. Brightness temperature simulations are obtained using the community radiative transfer model (*CRTM,Liu2012,*

TABLE II
ATMS SPECTRAL AND NOISE CHARACTERISTICS

Channel Frequency (GHz)	Spectral Resolution (MHz)	Instrument Noise (K)
23.80	270	0.25
31.40	180	0.31
50.3	180	0.37
51.76	400	0.28
52.80	400	0.28
53.596 ± 0.115	170	0.29
54.40	400	0.27
54.94	400	0.27
55.50	330	0.29
57.290344	330	0.43
57.290344 ± 0.217	78	0.56
57.290344 ± 0.3222 ± 0.048	36	0.59
57.290344 ± 0.3222 ± 0.022	16	0.86
57.290344 ± 0.3222 ± 0.010	8	1.23
57.290344 ± 0.3222 ± 0.0045	3	1.95
88.2	2000	0.29
165.5	3000	0.46
183.31 ± 7	2000	0.38
183.31 ± 4.5	2000	0.46
183.31 ± 3	2000	0.54
183.31 ± 1.8	2000	0.59
183.31 ± 1	2000	0.73

Moradi2020,Ding2011) for which new lookup tables for the appropriate transmittance coefficients were generated using the channel definitions in Table I. We use the Global Modeling and Assimilation Office (GMAO) GEOS version 5 (GEOS-5, [29]) Nature Run ([30] as the atmospheric truth for the brightness temperature simulations used in the sensitivity study and the retrieval performance validation shown next. This is a two-year global, nonhydrostatic mesoscale simulation from June 2005 to May 2007, gridded with a 7-km horizontal resolution. The atmospheric truth state X^T, used for the sensitivity study of Figs. 2–4 is a mid-latitude ocean profile extracted from this dataset. In Fig. 2, we used this truth profile X^T and, following the methodology, as in [38] and [31], we applied finite 1-K temperature perturbations in each 1-km-pressure layer to measure the finite response in brightness temperature in the oxygen bands. This response is commonly referred to as the temperature *sensitivity function*, also known as temperature *Jacobian*. The equivalent water vapor Jacobians for the water

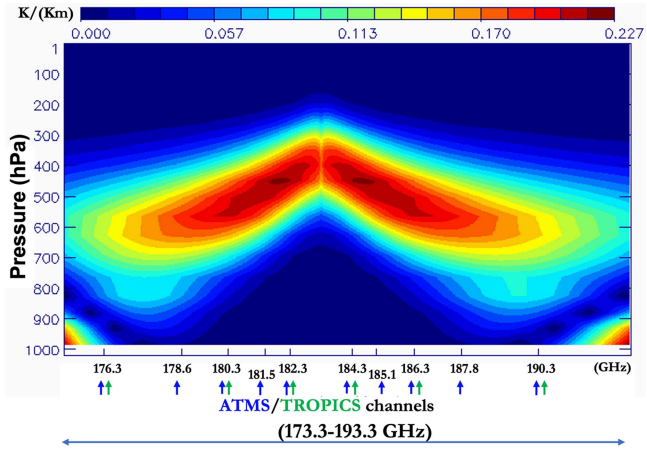

Fig. 3. Water vapor Jacobians in the 183 GHz spectral channels listed in Table I. A 5% water vapor perturbation in each 1-km-pressure layer of the atmospheric profile has been applied to measure the response in brightness temperature at each frequency of the 183-GHz water vapor band, using a 40-MHz spectral resolution. As for the temperature case, this figure illustrates the rich structure and high sensitivity to water vapor harnessed through a contiguous and high resolution spectral coverage of the microwave thermal spectrum, and largely missed from the sparse spectral sampling characterizing the program of record (blue and green arrows indicate the location of ATMS and TROPICS channels, respectively). Of particular relevance is the increased sensitivity in the mid/upper troposphere, where the highest impact on water vapor retrieval performance will be observed (see ahead, retrieval demonstrations).

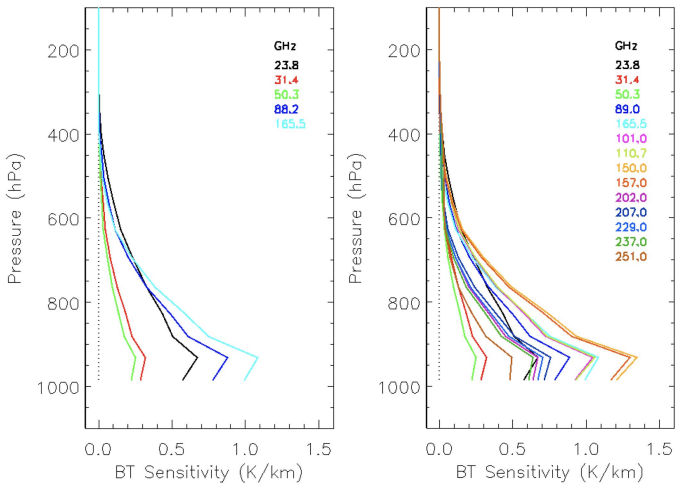

Fig. 4. Brightness temperature sensitivity to variations of water vapor in the window regions. 5% water vapor perturbations in each 1-km-pressure layer of the atmospheric profile have been applied to measure the response in brightness temperature in the window channels of ATMS (23.8, 31.4, 50.3, 88.2, 165.5 GHz, left figure) and a additional novel window channels (right figure) as listed in rows 4–25 of Table I. Functions are color-coded according to their associated frequency, displayed in the the top right corner of each figure. The most pronounced water vapor sensitivity functions are found in the 150-GHz region, followed by the 101 GHz, 110 GHz set, 165 GHz and the 200-GHz frequencies. As we shall see shortly, the novel higher frequency channels serve a critical role in improving water vapor retrieval performance in the lower troposphere (see ahead, retrieval demonstrations).

vapor and window channels listed in Table I are shown in Figs. 3 and 4, respectively. We obtained these curves by using the same reference state X^T, and applying 5% water vapor mixing ratio perturbations in each 1-km-pressure layer of the water vapor vertical profile. Since Jacobians are scene dependent—with

peaks shifting upward as atmospheric opacity increases [4]—we studied multiple geophysical scenarios and viewing geometries. An average from multiple latitudes would smooth out the fine vertical features of interest in this study. For this reason and for brevity, we only show a single, nadir looking, mid-latitude case as a representative test example.

Jacobians measure the thermal emission originating in each atmospheric layer of the discrete pressure grid, providing a measurement of the vertical sensitivity of the measurement with respect to a given species, in a given channel n ($n = 1,..., N$), centered on frequency ν. Ultimately, they play a central role in determining retrieval geophysical performance. Multiplied by the vertical derivative of the atmospheric transmittance, they form the row functions of the *radiative kernel matrix K*, in the radiative transfer equation (2). Here, (2) is obtained after discretization of the atmospheric column into L layers and linearization of the Planck function upon small perturbations ΔX_i, around the atmospheric truth state X_i^T, ($i = 1,..., L$), in each channel n. The far right side of (2) expresses the radiative transfer equation in matrix form

$$\Delta BT_n(\nu) = \sum_{i=1}^{L} K_{n,i} \cdot \Delta X_i \equiv K_{N,L} \cdot \Delta X_L. \tag{2}$$

The atmospheric pressure layering grid in CRTM is composed of $L = 100$ vertical levels and was selected to keep radiative transfer errors below the typical instrument noise characteristics of the current sensors from the program of record [32]. In the inverse problem, one would need the number of observations, i.e., the number of channels N, to be equal or greater than the number of unknowns L, forming the vertical grid of the retrieval profile, in order to invert (2) and obtain a fully resolved retrieval solution. The fundamental problem with current passive satellite sensors, however, is an ill-conditioned problem: even in the presence of a hyperspectral measurement (hundreds to thousands of N channel frequencies), errors in the measurement, lack of information content, and spectral correlation make the actual degrees of freedom in the measurement—the rank of the kernel matrix r—generally lower than the number of unknowns L. The lack of information content is exacerbated in the PBL, whose thermal emission signal is inherently absorbed by the overlaying layers of the middle and upper troposphere. Ill-conditioning has detrimental impact on geophysical retrieval quality and vertical resolution. Stabilization of the retrieval solution requires dependency on geophysical constraints which come at the expenses of regularization errors propagating into the retrieval solution.

Hyperspectral measurements are intended to mitigate the ill-conditioning problem present in the current thermal microwave program of record. Novel, higher resolution channels can offer improved signal to noise, information content, and vertical resolution in the vertical sounding of temperature and water vapor. Figs. 2 and 3 display the transpose matrices of the 60, 118, and 183-GHz temperature and water vapor Jacobians, respectively. The vertical axis reports the pressure in each layer i and the horizontal one the channel frequency ν, as listed Table I. This representation is meant to illustrate the rich vertical structure in the spectral sensitivity across the hyperspectral sampling of the microwave thermal domain, as we move from the core (upper troposphere/lower stratosphere peaking channels) to the pressure-broadened wings (PBL sensitive channels) of the oxygen and water vapor spectral lines. Blue and green arrows locate the frequencies in use by ATMS and TROPICS, which in contrast are sparse and of generally lower spectral resolution. An important goal of the study presented in this article is to assess what improvement over the program of record (e.g., ATMS), can be harnessed in the full exploitation of the microwave spectrum. Of particular interest, is the use of the full coverage in the spectral wings of the 60-GHz band, where the temperature Jacobians present significant strength and redundancy in the PBL. Similarly, we are interested in exploring what additional information content is harnessed in the 118-GHz band, which shows significant sensitivity in the middle- and upper troposphere temperature domain. Finally, we are interested in quantifying the water vapor retrieval impact derived from the full exploitation of the 183-GHz band and novel, unexplored window channels. Fig. 3 clearly indicates that a large part of the 183-GHz band is significantly underused in the current program of record, particularly in the middle and upper tropospheric sounding region. Fig. 4 is intended to investigate additional water vapor information content from the use of novel, unexplored channels in the window regions, carrying key information on the water vapor continuum. These are the channels listed in rows 4–25 of Table I, except those ones marked by asterisks. Given the high overlapping in the narrow region of the lower troposphere, for the sake of better visualization, we provide a simple over-plot of the vertical sensitivity functions. The novel water vapor sensitivity functions (right figure) show a more pronounced sensitivity to water vapor in the PBL region compared to the traditional ATMS 23.8, 31.4, 50.3, 89, and 165.5-GHz functions (left part). The most pronounced water vapor sensitivity functions are found in the 150-GHz region, followed by the 101 GHz, 110 GHz set, 165 GHz, and the 200 GHz frequencies. As we shall see shortly, these novel higher frequency channels serve a critical role in improving water vapor retrieval performance in the lower troposphere.

It must be said that in the infrared domain, temperature and water vapor sounding channels suffer from a large interference from atmospheric trace gases, requiring significant measurement thinning, [33]. In contrast, the thermal microwave only suffers from some negligible ozone interference [34]. Hence the increase in spectral coverage in the microwave domain is expected to more directly translate into improved signal-to-noise ratio and information content. Also, narrowing the spectral resolution inherently sharpens the Jacobians [4] and reduces the spectral correlation problem, which is expected to provide higher vertical resolution and more accurate retrieval profiles [35].

In the next section, we perform a quantitative analysis of the gain in retrieval sensitivity and vertical resolution as a result of the improved spectral coverage and resolution obtained using the hyperspectral configuration described in Table I.

B. Vertical Resolution and Retrieval Sensitivity Studies

The inverse solution of the radiative transfer (2) is expressed as

$$X_L^r = A_{L,L} \cdot X_L^T + (I_{L,L} - A_{L,L}) \cdot X_L^a \tag{3}$$

where A is given by the product of the so called *gain function* G, and the kernel matrix K, as described by (4). The gain function G, in turn, is expressed in terms of the kernel matrix K, normalized by the geophysical and measurement error covariance matrices and is a measure of the effective retrieval sensitivity to the measurement [36]

$$A_{L,L} = G_{L,N} \cdot K_{N,L}. \tag{4}$$

In inverse methods, A takes the name of *averaging kernel operator* [36] and provides a link between the retrieval solution X_L^r, the atmospheric truth X_L^T, and the geophysical a priori X_L^a. For simplicity, in (3), retrieval solution, truth, and geopysical a priori have been expressed on the same pressure grid of L layers, used in the previous derivation of Jacobians. Consequently, the A matrix in (3) and (4) has dimension $L \times L$ and so does I, the identity matrix. Due to ill-conditioning, however, retrievals are generally performed on coarser layers, to improve stability and save on computational time.

An important feature of (3) is the separation between the contribution to the retrieval solution originating from the actual measurement of the atmospheric truth, provided by A, and the contribution originating from the a priori, *(I - A)*. As explained in [36], in the ideal inverse method, the averaging kernel matrix would be the identity matrix I and the retrieval would return the truth, with full separation from the geophysical a priori. In practice, the rows of A, known as *averaging kernel functions*, are broad peaked functions, indicating that each vertical layer element of the retrieved solution, X_i^r ($i = 1,..., L$) is in reality an *average* quantity resulting from a sensitivity to changes in multiple vertical layers j ($j = 1,..., L$) of the true state, X_j^T. Another common way to express this concept is by saying that the overlaying layers of the retrieval solution are vertically correlated.

There are two equivalent ways to describe the physical meaning of the averaging kernel matrix and that are useful to retrieval performance assessment [35]. One is to say that each layer i of the retrieval solution is the result of a weighted average of the changes in all layers j of the true state vector, the weights being represented by the elements of the averaging kernel function of row index i (hence the definition of *averaging kernels functions*). The other is to say that a change in a given layer j of the true state gets smoothed out across multiple layers i of the retrieval state, the sensitivity to this perturbation being represented by the *jth* column elements of A (hence the name of *smoothing operator* also used for the A matrix). We can summarize these two concepts by saying that the row elements of A provide a measure of the effective vertical resolution of the retrieval solution and the column elements of A describe the effective vertical sensitivity of the retrieval solution to changes in the truth. The remaining contributions to the solution originate from the geophysical a priori and are similarly weighted by the elements of *I-A*.

In summary, the closer is A to the identity matrix, the lower is the solution dependency on the a priori and the higher is its sensitivity to the atmospheric truth. To that end, hyperspectral measurements serve the scope of improving the A matrix resemblance of the full identity matrix, in that increasing coverage and spectral resolution fills the vertical gaps and sharpens the Jacobians forming the Kernel matrix K, in (4). Also, any improvement in the sources of errors affecting the retrieval problem (e.g., instrument NeDT, forward model errors, etc.) will strengthen the gain function G in (4) and ultimately improve A. In this respect, instrument noise tolerance trade studies become equivalently important when designing a hyperspectral measurement sensor and will be the subject of our next study. Considerations on how hyperspectral microwave measurements can improve forward models will be discussed in Section IV.

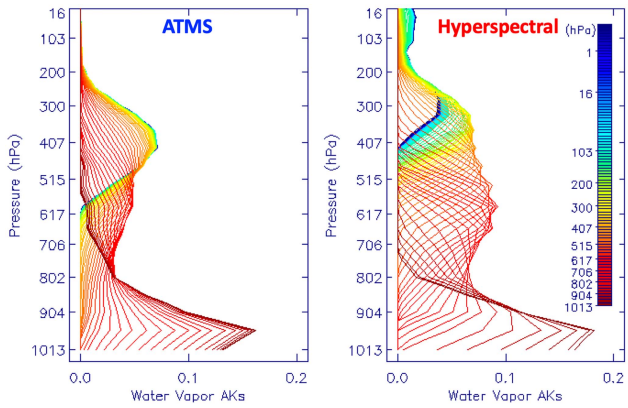

Fig. 5. Water vapor averaging kernel functions (*AKs*) from ATMS (left) and the hyperspectral configuration in Table I (right). The channel list used to build the ATMS water vapor A matrix are the five 183-GHz channels and the five window channels (23.8, 31.4, 50.3, 88.2, and 165.5 GHz) in Table II. For the hyperspectral case, we used all the 173.3–183.3 GHz and the window channels in rows 4–25 of Table I. Left part of Fig. 5 shows ATMS water vapor averaging kernel functions. Right side is for the hyperspectral configuration. The color table on the side of the figure reports the pressure values p_i, corresponding to each vertical layer i, $i = 1,..., L$, of the retrieval and truth pressure grid, in increasing order from near the top of the atmosphere (blue, layer index *1*, $p_1 = 0.01$ hPa), to the surface (red, layer index L and, in the current example, $p_L = 1013$ hPa). We use the same color code to plot the corresponding averaging kernel row functions A_i. While the ATMS averaging kernel functions show a high degree of overlapping, resulting in roughly three to four separable coarse layers, the hyperspectral configuration shows generally more pronounced, centered and narrow averaging kernel functions. Of particular interest is the improvement in the PBL, where a separation between two, more pronounced peaks can be observed.

An illustration of the improved features of A when using hyperspectral microwave measurements is provided in Fig. 5. We focus this study on the water vapor demonstration, comparing the A matrices from ATMS and the hyperspectral configuration. The channel list used to build the ATMS water vapor A matrix are the five 183-GHz channels and the five window channels (23.8, 31.4, 50.3, 88.2, and 165.5 GHz) in Table II. For the hyperspectral case, we used all the 173.3–183.3 GHz and the window channels in rows 4–25 of Table I. The left part of Fig. 5 shows ATMS water vapor averaging kernel functions. Right side is for the hyperspectral configuration. The color table on the side of the figure reports the pressure values p_i, corresponding to each vertical layer i, $i = 1,..., L$, of the retrieval and truth pressure grid, in increasing order from near the top of the atmosphere (blue, layer index *1*, $p_1 = 0.01$ hPa), to the surface (red, layer index L and, in the current example, $p_L = 1013$ hPa). We use the same color code to plot the corresponding averaging kernel row functions A_i. Here, the darkest blue curve, for example,

describes the elements of the very first row of A; the orange curve describes the elements of the row function for the pressure layer at 300 hPa and so on. If the problem was well posed, the one and only one solution in layer i, X_i^r, would be identical to X_i^T and its A_i would the a delta function. Instead, A_i includes nonzero contributions from multiple layers of the truth and, following [37], the full width at half of the maximum of the peak of A_i quantifies the effective vertical resolution of the retrieval solution at pressure p_i. Fig. 5 illustrates the generally overlapping and smoothed nature of the row functions of A. However, while the ATMS averaging kernel functions (left) show a high degree of overlapping, resulting in roughly three to four separable coarse layers, the hyperspectral configuration, on the other hand (right figure), shows generally more pronounced, centered, and narrow averaging kernel functions. A more distinct separation of the peaks can be observed along the full vertical extent, with a total of ten or more separable peaks. This confirms the expected results and is indicative of a generally higher retrieval sensitivity and vertical resolution, when hyperspectral measurements are used. The hyperspectral functions become significantly more pronounced and localized in the mid troposphere, filling the gap left by ATMS in this region. Of particular interest is also the improvement in the PBL, where a separation between two, more pronounced peaks can be observed. Both aspects are expected to lead to improved determination of PBL height. Next section examines more directly the impact on retrieval performance expected from the use of hyperspectral microwave data.

C. Retrieval Demonstrations

In this session, we assess the retrieval improvement that can be gained from an extended, hyperspectral coverage in the microwave thermal spectrum. The authors in [4] used the configuration described in Table I to assess the percentage error improvement over the geophysical a priori. We extend their work by performing an end-to-end retrieval performance analysis via rms and bias temperature and water vapor retrieval error statistics.

The retrieval processing system used in this study is an updated version of the combined atmospheric infrared sounder (AIRS)/AMSU retrieval method described in [38], expanded to run the community radiative transfer model (CRTM, [26]). In depth documentation on this retrieval method can be found in [38] and [39]. A brief summary is provided here for completeness.

This is an iterative, regularized, linearized least square minimization. At the core of this method is a sequential approach aimed at improving the linearization approximation of the radiative transfer equation. Since the Planck function is more linear in temperature, the first retrieval step solves for temperature. Once temperature is solved for, water vapor is solved next. This method has been proven successful in stabilizing the retrieval solution and relies on a proper channel selection and spectral correlation error characterization [33], [35], [38]. In this methodology, at each step, the spectral interference of the variable not solved for (e.g., water vapor during the temperature retrievals and, *viceversa*, temperature during the water vapor retrieval step), is treated as an off-diagonal spectral correlation error term of the measurement error covariance. During the temperature retrieval step, the correlation error is computed as the brightness temperature difference resulting from a 20% perturbation in the water vapor and cloud liquid water first guesses. During the water vapor retrieval, the correlation error is computed as the brightness temperature difference resulting from a perturbation in the temperature retrieval by the amount of its retrieval error estimate. The final measurement error covariance results in the summation of three terms: the instrumental noise term, the error resulting from a combination of calibration errors, and errors in the radiative forward model and, finally, the spectral correlation error. The instrument noise specifications are those provided in Tables I and II. The radiative transfer model error is set equal to 1 K for all channels. We added a constant 0.1 K term to represent additional sources of errors that are not measurable at this time (e.g., calibration and representativeness errors).

Simulated ATMS and hyperspectral microwave data were generated using the CRTM forward model. As truth for the forward model simulation and the retrieval demonstration, we used the GMAO GEOS-5 Nature Run. For the regularization of the retrieval solution, we used the GMAO GEOS-5 Nature Run initialization state. In Figs. 6 and 7, results are shown in the form of rms (left two figures) and bias statistics (right two figures) of temperature and water vapor retrievals. The dataset used for this retrieval demonstration spans an ensemble of global, ocean, clear-sky scenes from August 15th, 2003 of the GMAO GEOS-5 Nature Run. Hyperspectral retrievals statistics are compared against equivalent ATMS (blue curves) and first guess (black curves) retrievals. For simplicity, we will refer from now on to ATMS as the *baseline*. We parse our experiments into incremental steps and study the impact on retrieval performance resulting from different configurations, each reflecting specific technology design solutions, all intended to maximize retrieval performance within SWaP-C constraints.

1) Experiment I: Comprehensive Hyperspectral Coverage: Our first experiment is intended to assess the retrieval improvement that can be gained from a comprehensive coverage of the spectral configuration introduced in Table I.

As a first step, we use the ATMS baseline configuration and replace its five water vapor sounding channels (last five rows in Table II) with the hyperspectral water vapor channel set (third row in Table I). This new set is composed of 500 channels spanning the 173.3–193.3-GHz band, with a spectral resolution of 40 MHz. Water vapor rms and bias error statistics upon the addition of this hyperspectral water vapor channel set are illustrated by the orange curve in Fig. 6. An up to ∼40% improvement with respect to the baseline (blue curve), is observed in the middle and upper troposphere water vapor statistics. The slight degradation observed in the lower troposphere may be the result of an imbalance introduced by the use of hundreds of similar channels. We performed a separate test (not shown for brevity), where some lower tropospheric sensitive channels were removed from the hyperspectral list and obtained an improved result in the lower troposphere, compared to ATMS.

Our second step uses Step 1 configuration as a new starting point. We replace ATMS temperature sounding channels (rows

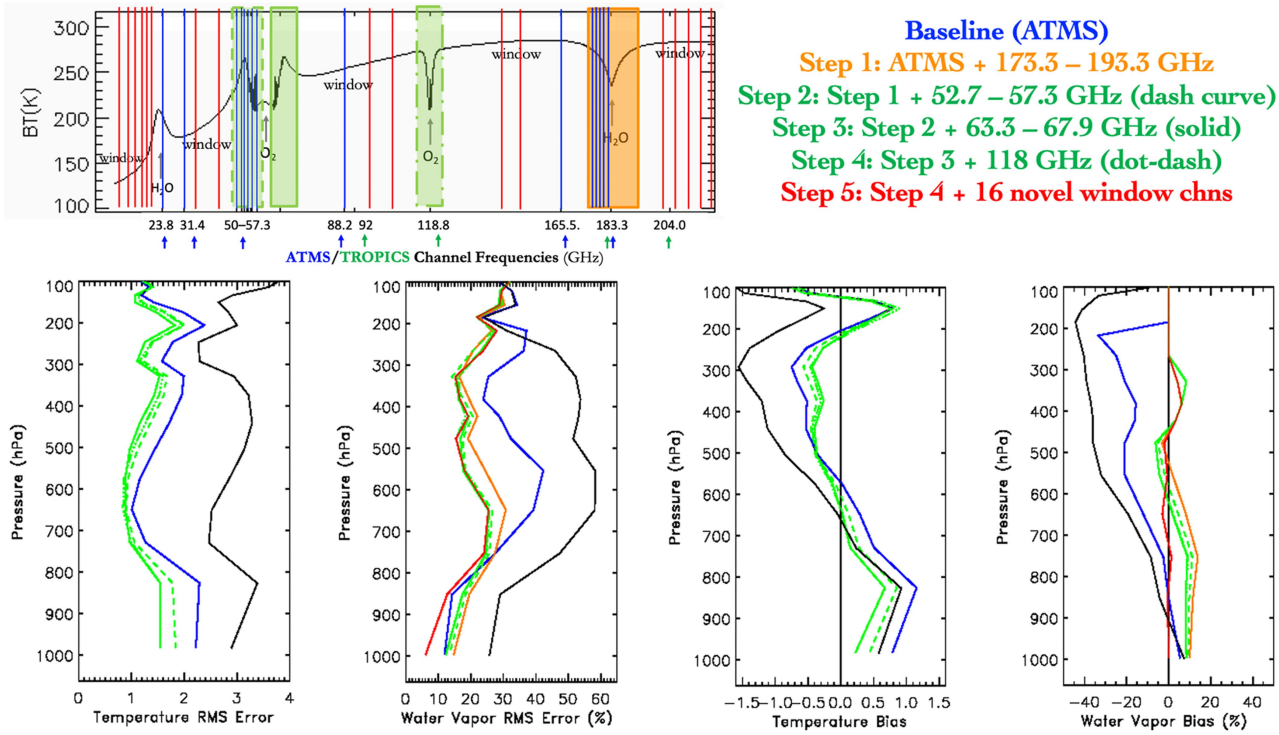

Fig. 6. Experiment I: Comprehensive hyperspectral coverage. Experiment I provides an overview of the gain in retrieval performance obtained from full, hyperspectral utilization of the thermal microwave spectrum via incremental data addition steps. Baseline configuration: ATMS channel list in Table II and indicated by blue bars in the top left figure. Step 1: Replacement of five ATMS 183-GHz water vapor channels with 500 hyperspectral water vapor channels from the 173.3–193.3-GHz region (Table I third row, orange box in upper left figure). Statistical results are represented by orange curves in the bottom figures of the water vapor rms and bias statistics. Step 2: Replacement of eleven ATMS 52.8–57-GHz temperature sounding channels with the hyperspectral 52.6–57.3-GHz temperature sounding channels (Table I first row, dash-contoured green box in upper left figure). Statistical results are represented by dash green curves in the bottom figures of the temperature and water vapor rms and bias statistics. Step 3: Addition of the hyperspectral 63.3–67.9-GHz temperature sounding channels (Table I first row, solid-contoured green box in upper left figure). Statistical results are represented by solid green curves in the bottom figures of the temperature and water vapor rms and bias statistics. Step 4: Addition of the hyperspectral 118-GHz temperature sounding channels (Table I second row, dash-dot-contoured green box in upper left figure). Statistical results are represented by dash-dot green curves in the bottom figures of the temperature and water vapor rms and bias statistics. Step 5: Addition of novel window channels (Table I, rows 4–25 except channels marked by one asterisk, which are already in the ATMS channel set. Those are marked as red bars in upper left figure). Statistical results are represented by red curves in the bottom figures of the water vapor RMS and bias statistics. Hyperspectral retrievals statistics are compared against equivalent results from ATMS (blue curves) and from the retrieval first guess (black curves). The data set used for this retrieval demonstration spans an ensemble of global, ocean, clear-sky scenes from August 15th, 2003 of the GMAO GEOS-5 Nature Run.

5–15 in Table II) with the hyperspectral 52.6–57.3-GHz channel list, sampled with a spectral resolution of 10 MHz (first row in Table I). Results are shown by the green dash curves in Fig. 6. Second, we add the remaining 63.3–67.9-GHz band (also sampled with 10-MHz resolution) and show results using the solid green curves also in Fig. 6. As a third step, we add the 113.7–123.7-GHz band (second row in Table I, 20-MHz resolution). Results are shown by the dash-dot green curves in Fig. 6. The use of the 52.6–57.3-GHz hyperspectral line alone provides a noticeable improvement along the full atmospheric column, in both rms and bias temperature statistics (dash green versus blue). The incremental addition of the remaining 63.3–67.9-GHz channels is observed to further improve the temperature statistical performance, particularly in the PBL. This is an important aspect in that it provides an indication of the improved signal to noise that can be derived from the full exploitation of the primary oxygen line. As expected from the sensitivity analysis, the addition of the 118-GHz line provides an improvement in the upper reaches of the atmosphere. Finally, it must be noted that improvements are observed not only in the temperature but also in the water vapor statistics. This aspect originates from the sequential order of the two retrieval steps, where the temperature retrieval acts as a background for the water vapor retrieval. As such, any improvement in temperature is often consistently reflected in an improvement in water vapor performance.

We complete this first experiment by testing the addition of novel window channels to the water vapor retrieval channel list (rows 4 to 25 in Table I not marked by an asterisk). Results are shown by the red curves of the water vapor statistics in Fig. 6. These novel window channels are observed to provide an additional ∼10% improvement in the water vapor rms and bias performance (now ∼50% better than the baseline), particularly in the PBL (red versus orange and blue curves). This result confirms the value of extending the coverage in the microwave window bands toward improved sensitivity to water vapor, particularly in the boundary layer. Future studies will examine land scenarios for which the role of extended window coverage is key to improved retrieval of surface properties (classification, surface temperature).

In summary, the final configuration of experiment I—a comprehensive use of hyperspectral sampling in the temperature and

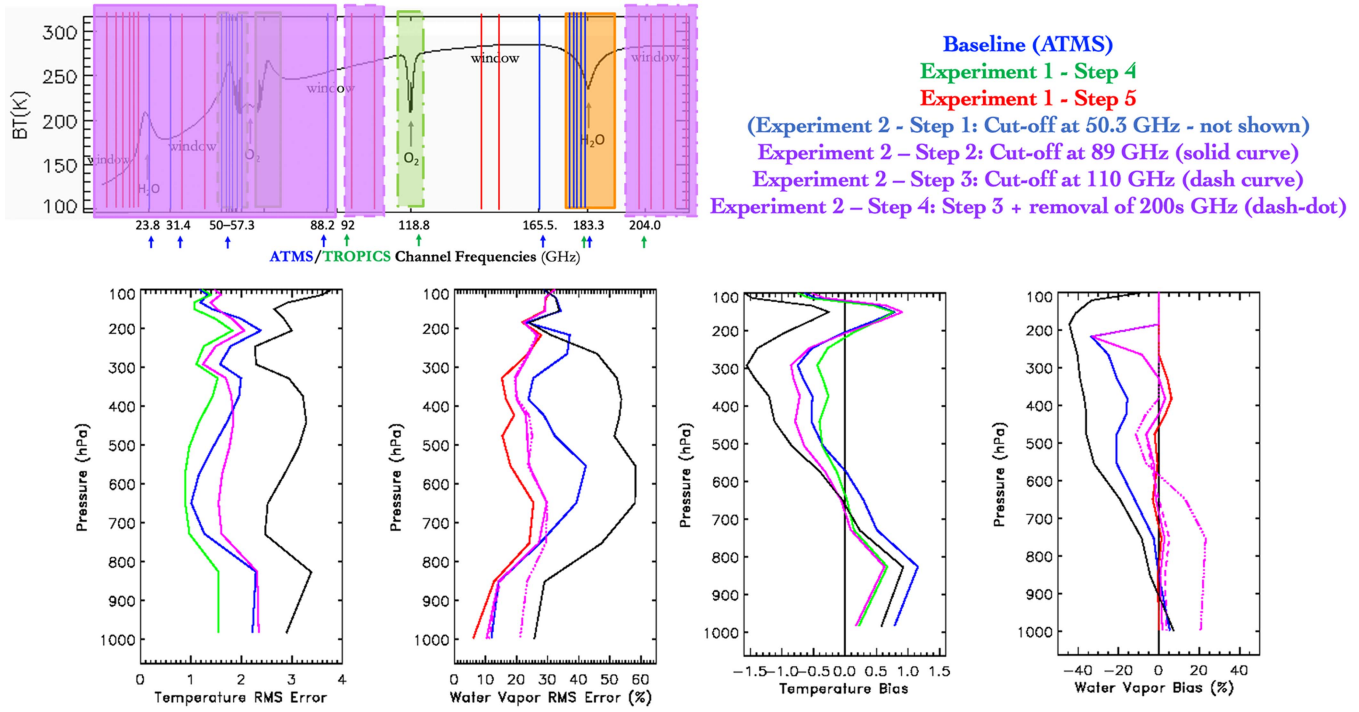

Fig. 7. Experiment II: Lower versus higher frequencies of the microwave domain. Experiment II performs a few data denials in the low frequency domain and tests the resulting penalization in retrieval performance. Step 1: Removal of the lowest window channels frequencies (6.92 GHz to 50.3 GHz, Table I, rows 4 - 11). Statistical results are not shown because indistinguishable from Experiment I configuration. Step 2: Incremental removal of all channels up to 89 GHz (solid purple box in upper left figure). Statistical results are represented by purple solid curves in the bottom figures of the temperature and water vapor rms and bias statistics. Step 3: Incremental removal of all channels up to 110 GHz (dash purple box in upper left figure). Statistical results are represented by purple dash curves in the bottom figures of the temperature and water vapor rms and bias statistics. Step 4: Incremental removal of all channels higher than 200 GHz (dash-dot purple box in upper left figure). Statistical results are represented by purple dash-dot curves in the bottom figures of the temperature and water vapor rms and bias statistics. Hyperspectral retrievals statistics are compared against equivalent results from ATMS (blue curves) and from the retrieval first guess (black curves). The dataset used for this retrieval demonstration spans an ensemble of global, ocean, clear-sky scenes from August 15th, 2003 of the GMAO GEOS-5 Nature Run.

water vapor lines, along with an improved coverage in all the window regions—stands out as the best performing system. Our experiment shows an overall rms and bias improvement of up to 50% and 25% in the PBL and free tropospheric temperature, respectively, compared to the baseline (solid green versus blue). The water vapor field is observed to undergo a significant improvement as well. The water vapor rms error is observed to improve by about 50% in the PBL and along the full extent of the free troposphere with respect to the baseline (solid red versus blue curves). It must be said, that the GMAO GEOS-5 Nature Run first guess presents already a relatively good performance in the PBL water vapor field (black curve). However, the hyperspectral configuration is capable of correcting the shape of its bias statistics, bringing it to a nearly flat zero value, throughout the entire extent of the PBL. This feature is indicative of high retrieval skill in this region. Both improvements, in the PBL and free troposphere temperature and water vapor, are expected to benefit the identification of PBL height. We will use the configuration of Experiment I as a new starting point for a second experiment.

2) Experiment II: Lower Versus Higher Frequencies of the Microwave Domain: Efficient SWaP-C is one of the major concerns in space-borne hyperspectral microwave technology. As the size of the receiver antenna increases with smaller frequencies, it is useful to assess the impact on product performance resulting from the possible removal of some low frequency channels from the retrieval channel list. This experiment is devoted to this scope. A focus of this study is the use of novel, higher frequency channels as a means for compensating the loss of low frequency ones, so as to find an optimal tradeoff between SWaP-C and product performance. We use the final configuration from experiment I as a starting point to test a few data denial scenarios affecting the low-frequency domain. As a first step—not shown for visualization clarity—we start from the lowest window channel frequency in Table I (6.92 GHz) and incrementally remove all remaining window channels up to the 50-GHz window channel (rows 4–11 in Table I). No noticeable degradation is observed in the retrieval performance. This result can be explained by the clear-sky, ocean only nature of this experiment and the role played by the higher frequency window channels in preserving the retrieval quality. In step two and three, we test two additional drop-off thresholds, 89 and 110 GHz. Results are illustrated by the purple solid and dash curves, respectively, in Fig. 7. The whole 60-GHz oxygen line has been removed along with all the lower frequency window channels up to the thresholds (thresholds excluded as well).

The 89-GHz cutoff configuration can be interpreted as a hyperspectral version of the TROPICS radiometer, augmented by the use of novel (i.e., non-ATMS) higher frequency window channels and a hyperspectral coverage in the 118 and 183 GHz

lines. The 110-GHz cutoff configuration is a possible solution for the future atmospheric observing system radiometers [40]. Solid and dash purple curves are indistinguishable. The penalty of losing the low window channel frequencies and the 60-GHz band is visible in the mid-tropospheric temperature rms and bias results (solid and dash purple versus green curves). The water vapor rms and bias performance is still better than the baseline, thanks to the hyperspectral sampling in the 183-GHz line but shows a visible degradation (up to 5%) with respect to the configuration of experiment I (solid and dash purple versus red). In conclusion, the retrieval performance does not appear severely compromised by the removal of the low-frequency channels. This result, however, reflects two important aspects. First, this is an ocean, clear sky only demonstration. The role of the low-frequency channels in the presence of clouds and over more complex land scenes will be investigated in a follow up study. Second, the novel high-frequency window channels (202, 207, 229, and 251 GHz) play a key role in preserving the water vapor retrieval quality. We illustrate this result by removing these channels from the water vapor channel list in our third and final step of this second experiment. Results are represented by the dot-dash curve in the water vapor statistics of Fig. 7, indicating an up to 20% rms and bias degradation resulting in the PBL water vapor statistical performance.

The conclusion we draw from this second experiment is that increased coverage in the higher frequency domain is key to compensate for the loss of the low-frequency domain, should this design become necessary to maintain efficient SWaP-C.

III. State of the Art in Space Borne Hyperspectral Microwave Technology

The critical technology elements for microwave hyperspectral sounder technology include wideband radio frequency (RF) front-ends (RFE), filterbanks, and spectrometers. The specifications for application of each of these technologies will vary based on instrument architecture and be driven by science requirements and technical capability. The wideband RFE provides calibration source and prepares the microwave signals for processing to produce a measured spectrum. Radio frequency integrated circuit (RFIC) and monolithic microwave integrated circuit (MMIC) technology continually advances to enable ever-increasing bandwidths in amplifiers and mixers, which has driven designs for broadband matching networks. These technologies are the basis of total power or correlation radiometer front ends. However, hyperspectral architectures need not accept the entire spectrum into a solitary receiver and are likely to divide the spectrum into more digestible portions. Such receivers are likely to include heterodyne stages to down-convert bands to lower intermediate frequencies or even to baseband. Nevertheless, perhaps more important and certainly an enabling technology is that of spectrum analysis processing. Different approaches from the past include analog filterbanks, digital signal processing (DSP)-based spectrometers, and acousto-optical spectrometers (AOS). Analog approaches are typically limited to no more than a few tens of channels (e.g.,*Waters2006,Magalhaes*). For hyperspectral to reach hundreds or even thousands of channels, other approaches

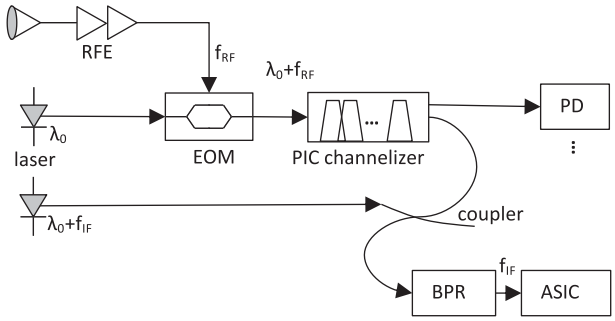

Fig. 8. Simplified block diagram of the microwave photonics spectrometer. Microwave signals enter the antenna (upper left) and are prepared by the RF front-end (RFE) for the electro-optic modulator (EOM). The EOM is driven by a laser to generate the RF spectrum on the optical carrier. A photonic-integrated circuit (PIC) channelizer divides the RF spectrum into multiple, neighboring bands. Only two output bands are shown for simplicity. One band's power can be detected by a photodetector while another is downconverted by highspeed photoreceiver driven by an offset frequency laser. The downconverted band is processed by an ASIC digital spectrometer.

are required. Before digital circuits were capable, AOS technology was exploited, [50]. However, digital processing is preferred generally for stability, size, and power dissipation. FPGA-based filterbanks have found utility in radio-frequency interference detection [51], [52], [53], [54].

A. Emerging Technology

A combination of digital application specific integrated circuit (ASIC) and microwave photonics has emerged as a new architecture for hyperspectral microwave sounding (Fig. 8). Microwave photonics are used to convert tens of GHz of microwave RF or IF signals to infrared wavelengths, drastically reducing the fractional bandwidth of the received signals. Preliminary results demonstrate the feasibility of this photonic approach [55], [56]. Photonic integrated circuits (PICs) are used to divide the wideband spectrum into narrower channels, which would previously have been done using RF or IF filters. These smaller channels can be treated as total power channels using photodectors (as opposed to RF detectors), or down-converted to a secondary IF and processed digitally. Instead of using FPGA's, high-resolution digital spectrometers implemented in radiation-tolerant digital ASICs promise multi-GHz bandwidths covered by thousands of channels ([57]).

Software-defined bandpass responses are created using the high-resolution spectral data. Combining PIC and ASIC—*PICASIC*—technology can create a modular approach to processing broad, contiguous regions of the microwave spectrum and is currently being developed for the hyperspectral microwave photonic instrument (HyMPI) [58], [59]. The *PICASIC* modular approach enables full-spectrum and contiguous spectral coverage of Earth's microwave thermal radiation, with a selectable capability to measure the spectrum with higher resolution where unique information content in the signal is exhibited. To this end, the PICASIC can enable the first of its kind combined hyperspectral microwave imager and sounder within feasible SWaP-C constraints, suitable to meet the requirements of the next generation of hyperspectral microwave satellite sensors [58], [59].

IV. Conclusion

Recent advances in sensor component technology have allowed hyperspectral microwave sounding to become a realistic and cost-effective possibility. To that end, assessing the information content that can be gained from the various bands of the thermal microwave spectrum is important toward informing the engineering and technology decisions that will ultimately lead to the next generation of hyperspectral microwave sensors from space.

This work presented a comprehensive sensitivity analysis of the full thermal microwave domain. We performed an end-to-end temperature and water vapor retrieval demonstration with a particular focus on quantifying and comparing the impact on retrieval performance resulting from specific bands and channels, by means of data addition and denial trade studies. In doing so, we assessed different spectral configurations, each reflecting specific technology solutions intended to obtain improved geophysical product performance within feasible SWaP-C constraints. Our results (Fig. 6) indicate that a comprehensive use of hyperspectral sampling in the temperature and water vapor lines, along with an improved coverage in all the window regions, stands out as the best performing design. Our experiments show that the use of hyperspectral sampling in the sounding lines alone can provide improvements in the PBL and free tropospheric thermodynamic fields of up to ∼40%, when compared against the program of record performance. Our experiments also demonstrated the essential role played by an improved coverage in the window regions so as to augment information content in the water vapor continuum, leading to an overall improvement of up to ∼50% in the PBL. The *PICASIC* technology described in Section III promises to enable this contiguous, hyperspectral coverage capability of the thermal microwave spectrum, within suitable SWAP-C specifications, suitable for space deployment.

The observed improvements in atmospheric thermodynamic sounding obtained from these hyperspectral microwave measurements will be critical to enhance numerous driving applications that are important to climate science and NWP [2]. A few of those are outlined in the following.

Of particular interest will be the utilization of hyperspectral microwave measurements in combination with other passive (e.g., hyperspectral infrared, global navigation satellite system radio occultation) and active measurements (e.g., lidar and radar), as envisioned by the NASA PBL Incubation Study Team report [6]. To that end, hyperspectral microwave soundings of the quality demonstrated in Fig. 6, are expected to help improve depiction of the thermodynamic structure of the PBL, so as to address each of the critical PBL science questions outlined in the PBL Study Team Report Science and Application Traceability Matrix (SATM) [6].

Enhanced thermodynamic soundings like those observed in Fig. 6 are expected to significantly benefit tropical cyclone intensification forecast, whose accuracy relies upon knowledge of the temperature and moisture field within and around the storm core ([41], [42], [43]). Rapidly updated humidity fields provided by a Smallsat/Cubesat constellation of hyperspectral microwave sensors will provide accurate atmospheric motion vectors, to help filling the gap in mid-tropospheric winds, left by the current program of record [44].

Increased sampling and spectral resolution will be key to detect the ever growing RF interference (RFI) from incumbent active services, particularly 5G and 6G networks, which has become an element of serious concern. RFI presents a high, hard-to-predict variability in space and time and the noise introduced in the measurement has been shown detrimental on temperature and precipitation forecasting [45]. With 6G interfering signals now affecting the whole 50-GHz region, high spectral resolution and low noise characteristics, as those in Table I, along with the utilization of novel frequencies outside the traditional passive allocated microwave spectrum, become necessary to the detection of RFI signals. Also, a software-programmable capability will be critical to enable spectral response functions (SRFs) matched to any legacy sounder, for intercomparison and cross-calibration.

Improved spectral resolution and coverage will also prove beneficial to the fundamental understanding of atmospheric microwave spectroscopy. Some of the known issues in current microwave radiative transfer models, include uncertainties in surface emissivity models, especially over land [27], uncertainties in the spectral absorption line shapes and positions [46], and uncertainties in the water vapor continuum [47]. Lack of high spectral resolution measurements in the microwave thermal domain has been one of the limiting factors in making advancements in these areas. First of a kind contiguous, high resolution measurements will provide a unique and unprecedented opportunity to investigate these issues, which, when corrected, will lead to critical improvements in radiative transfer, data assimilation applications, and support new discoveries in atmospheric physics.

The work presented here focused on ocean, clear-sky demonstrations. Future work will extend this analysis to more complex cloud and surface types, as we advance our capability to simulate more complex scenarios and improve scene variability. A fundamental part of this work will be represented by noise tolerance studies as the first hyperspectral microwave sensor prototypes approach maturity. This work will prove essential in preparation for upcoming airborne field campaign demonstrations of hyperspectral microwave observations, the first stepping stone ultimately leading to the next generation of space borne hyperspectral microwave sensors.

Acknowledgment

The authors would like to thank the reviewers for the valuable suggestions offered to improve the manuscript.

References

[1] W. J. Blackwell et al., "Hyperspectral microwave atmospheric sounding," *IEEE Trans. Geosci. Remote Sens.*, vol. 49, no. 1, pp. 128–142, Jan. 2011.
[2] S. A. Boukabara and K. Garret, "Benefits of a hyperspectral microwave sensor," in *Proc. IEEE Sensors*, 2011, pp. 1881–1884.
[3] J-F. Mahfouf, C. Birman, F. Aires, C. Prigent, E. Orlandi, and M. Milz, "Information content on temperature and water vapour from a hyperspectral microwave sensor," *Quart. J. Roy. Meteorological Soc.*, vol. 141, pp. 3268–3284, 2015, doi: 10.1002/qj.2608.

[4] F. Aires et al., "Microwave hyperspectral measurements for temperature and humidity atmospheric profiling from satellite: The clear-sky case," *J. Geophys. Res. Atmospheric*, vol. 120, pp. 11,334–11,351, 2015.

[5] F. Aires, C. Prigent, S. Buehler, and P. Eriksson, "Towards more realistic hypotheses for the information content analysis of cloudy/precipitating situations – Applications to a hyperspectral instrument in the microwave," *Quart. J. Roy. Meteorological Soc.*, vol. 145, no. 718, pp. 1–14, 2019.

[6] J. Teixeira et al., "Toward a global planetary boundary layer observing system: The NASA PBL incubation study team report," NASA PBL Incubation Study Team, NASA, Washington, DC, USA, Tech. Rep., 2021, p. 134. [Online]. Available: https://science.nasa.gov/science-pink/s3fspublic/atoms/files/NASAPBLIncubationFinalReport2.pdf

[7] P. Bauer, G. Ohring, C. Kummerow, and T. Auligne, "Assimilating satellite observations of clouds and precipitation into NWP models," *Bull. Amer. Meteorological Soc.*, vol. 92, no. 6, pp. ES25–ES28, 2011.

[8] A. J. Geer, "All-sky assimilation: Better snow-scattering radiative transfer and addition of SSMIS humidity sounding channels," Eur. Centre Medium-Range Weather Forecasts, Reading, U.K., Tech. Rep. 706, 2009.

[9] C. Cardinali, "Forecast sensitivity to observation as a diagnostic tool," Eur. Centre Medium-Range Weather Forecasts, Reading., U.K., Tech. Rep. 599, 2009.

[10] G. Radnoti, P. Bauer, A. McNally, C. Cardinali, S. Healy, and P. De Rosnay, "ECMWF study on the impact of future developments of the space-based observing system on Numerical Weather Prediction," Eur. Centre Medium-Range Weather Forecasts, Reading., U.K., Tech. Rep. 638, 2010.

[11] A. C. Lorenc and R. T. Marriott, "Forecast sensitivity to observations in the Met Office Global numerical weather prediction system," *Quart. J. Roy. Meteorological Soc.*, vol. 140, no. 678, pp. 209–224, 2014.

[12] R. Gelaro, R. H. Langland, S. Pellerin, and R. Todling, "The THORPEX observation impact intercomparison experiment," *Monthly Weather Rev.*, vol. 138, no. 11, pp. 4009–4025, 2010.

[13] Y. Zhu, R. Todling, and N. Arnold, "Observation impact and information retention in the lower troposphere of the GMAO GEOS data assimilation system," *Monthly Weather Rev.*, vol. 150, no. 8, pp. 2187–2205, 2022.

[14] E-S. Chung, B. Soden, B. J. Sohn, and L. Shi, "Upper-tropospheric moistening," *Proc. Nat. Acad. Sci.*, vol. 111, pp. 11636–11641, Aug. 2014, doi: 10.1073/pnas.1409659111.

[15] C-Z. Zou, W. Wang, J. Li, Jian, and NOAA CDR Program, "NOAA climate data record of microwave sounding unit (MSU) and advanced microwave sounding unit (AMSU-A) mean layer temperature, version 3.0," NOAA Nat. Centers Environ. Inf., Ashville, NC, USA, 2015, doi: 10.7289/V5QF8QTK.

[16] F. Weng, X. Zou, X. Wang, and M. D. Goldberg, "Introduction to Suomi national polar-orbiting partnership advanced technology microwave sounder for numerical weather prediction and tropical cyclone applications," *J. Geophys. Res.: Atmospheres*, vol. 117, no. D19, 2012, doi: 10.1029/2012JD018144.

[17] W. J. Blackwell et al., "An overview of the TROPICS NASA Earth venture mission," *Quart. J. Roy. Meteorological Soc.*, vol. 144, no. S1, pp. 16–262018.

[18] V. Mattioli et al., "The EUMETSAT polar system - second generation (EPS-SG) passive microwave and sub-mm wave missions," in *Proc. Photon. Electromagn. Res. Symp.-Spring*, 2019, pp. 3926–3933.

[19] T. Lupi et al., "MicroWave imager for MetOp-SG: Development status and instrument verification," in *Proc. 16th Specialist Meeting Microw. Radiometry Remote Sens. Environ.*, 2020, pp. 1–4.

[20] P. W. Rosenkranz, "Water vapor microwave continuum absorption: A comparison of measurements and models," *Radio Sci.*, vol. 33, pp. 919–928, .

[21] A. Lipton, "Satellite sounding channel optimization in the microwave spectrum," *IEEE Trans. Geosci. Remote Sens.*, vol. 41, no. 4, pp. 761–781, Apr. 2003.

[22] P. Bauer and S. Di Michele, "Study on definition of mission requirements for a post-EPS microwave radiometer for cloud and precipitation observation," ECMWF, Reading, U.K., EUMETSAT Cntract EUM/CO/O6/1510/PS, 2007.

[23] B. Lambrigsten, S. T. Brown, T. C. Gaier, L. Herrell, P. P. Kangaslahti, and A. B. Tanner, "Monitoring the hydrologic cycle with the PATH mission," *Proc. IEEE.*, vol. 98, no. 5, pp. 862–877, May 2010.

[24] C. D. Kummerow et al., "Hyperspectral microwave sensors—Advantages and limitations," *IEEE J. Sel. Topics Appl. Earth Observ. Remote Sens.*, vol. 15, pp. 764–775, 2022.

[25] E. Kim, C.-H. J. Lyu, K. Anderson, R. V. Leslie, and W. J. Blackwell, "S-NPP ATMS instrument prelaunch and on-orbit performance evaluation," *J. Geophys. Res.: Atmospheres*, vol. 119, no. 9, pp. 5653–5670, 2014.

[26] Q. Liu et al., "Community radiative transfer model for radiance assimilation and applications," in *Proc. IEEE Int. Geosci. Remote Sens. Symp.*, 2012, pp. 3700–3703.

[27] I. Moradi et al., "Performance of radiative transfer models in the microwave region," *J. Geophysical Res.: Atmospheres*, vol. 125, 2020, Art. no. e2019JD031831.

[28] Ding et al., "Validation of the community radiative transfer model," *J. Quant. Spectrosc. Radiative Transfer*, vol. 112, no. 6, pp. 1050–1064.

[29] M. M. Rienecker et al., "The GEOS-5 data assimilation system—Documentation of versions 5.0.1, 5.1.0, and 5.2.0," NASA, Washington, DC, USA, Tech. Rep. NASA/TM-2008-104606-VOL-27, 2008.

[30] R. Gelaro et al., "Evaluation of the 7-km GEOS-5 nature run," NASA, Washington, DC, USA, Tech. Rep. GSFC-E-DAA-TN21523, 2014.

[31] A. Gambacorta, "The NOAA unique combined atmospheric processing system (NUCAPS) algorithm theoretical basis document," Version 1.0, Nat. Ocean. Atmospheric Admin., Washington, DC, USA, Aug. 21, 2003. [Online]. Available: https://www.ospo.noaa.gov/Products/atmosphere/soundings/nucaps/docs/NUCAPS_ATBD

[32] L. L. Strow, S. E. Hannon, S. De Souza-Machado, H. E. Motteler, and D. Tobin, "An overview of the AIRS radiative transfer model," *IEEE Trans. Geosci. Remote Sens.*, vol. 41, no. 2, pp. 303–313, Feb. 2003.

[33] A. Gambacorta, "Methodology and information content of the NOAA/NESDIS operational channel selection for infrared hyper spectral sounders," *IEEE Geos. Remote Sens. Lett.*, vol. 51, no. 6, pp. 3207–3216, Jun. 2013.

[34] V. John and S. Buehler, "The impact of ozone lines on AMSU-B radiances," *Geophys. Res. Lett.*, vol. 31, no. 21, 2004, doi: 10.1029/2004GL021214.

[35] A. Gambacorta, "Atmospheric soundings from hyperspectral satellite observations," in *Comprehensive Remote Sensing*, S. Liang Eds., Amsterdam, The Netherlands: Elsevier., 2018, pp. 64–96.

[36] C. D. Rodgers, *Inverse Methods for Atmospheric Sounding*. Singapore: World Scientific, 2000.

[37] G. Backus and F. Gilbert, "Uniqueness in the inversion of inaccurate gross Earth data," *Philos. Trans. Roy. Soc. London. Ser. A., Math. Phys. Sci.*, vol. 266, no. 1173, pp. 123–192, 1970.

[38] J. Susskind, C. D. Barnet, and J. M. Blaisdell, "Retrieval of atmospheric and surface parameters from AIRS/AMSU/HSB data in the presence of clouds," *IEEE Trans. Geosci. Remote Sens.*, vol. 41, no. 2, pp. 390–409, Feb. 2003.

[39] J. Susskind, J. Blaisdell, L. Iredell, and F. Keita, "Improved temperature sounding and quality control methodology using AIRS/AMSU data: The AIRS science team Version-5 retrieval algorithm," *IEEE Trans. Geosci. Remote Sens.*, vol. 49, no. 3, pp. 883–907, Mar. 2011, doi: 10.1109/TGRS.2010.2070508.

[40] National Academies of Sciences, Engineering and Medicine (NASEM), "2017-2027 Decadal survey for Earth Science and Applications from Space (ESAS 2017) Thriving on Our Changing Planet: A Decadal Strategy for Earth Observation from Space," The National Academies Press. Washington, DC, USA, 2018.

[41] R. Gall, J. Franklin, F. Marks, E. N. Rappaport, and F. Toepfer, "The hurricane forecast improvement project," *Bull. Amer. Meteor. Soc.*, vol. 94, no. 3, pp. 329–343, 2013.

[42] D. Tao and F. Zhang, "Effect of environmental shear, sea-surface temperature, and ambient moisture on the formation and predictability of tropical cyclones: An ensemble-mean perspective," *J. Adv. Model. Earth Syst.*, vol. 6, pp. 384–404, 2014.

[43] Z. Pu and L. Zhang, "Validation of atmospheric infrared sounder temperature and moisture profiles over tropical oceans and their impact on numerical simulations of tropical cyclones," *J. Geophys. Res.*, vol. 115, 2010, Art. no. D24.

[44] D. McCarty, I. Carvalho, and N. Moradi Privé, "Observing system simulation experiments investigating atmospheric motion vectors and radiances from a constellation of four - five micron infrared sounders," *J. Atmospheric Ocean. Technol.*, vol. 38, no. 2, pp. 331–347, 2020.

[45] M. Yousefvand, C. -T. M. Wu, R. -Q. Wang, J. Brodie, and N. Mandayam, "Modeling the impact of 5G leakage on weather prediction," in *Proc. IEEE 3rd 5G World Forum*, 2020, pp. 291–296.

[46] H. Brogniez et al., "A review of sources of systematic errors and uncertainties in observations and simulations at 183 GHz," *Atmospheric Meas. Tech.*, vol. 9, pp. 2207–2221, 2016.

[47] F. J. Wentz and T. Meissner, "Atmospheric absorption model for dry air and water vapor at microwave frequencies below 100 GHz derived from space-borne radiometer observations," *Radio Sci.*, vol. 51, pp. 381–391, 2016.
[48] J. Waters et al., "The Earth observing system microwave limb sounder (EOS MLS) on the aura satellite," *IEEE Trans. Geosci. Remote Sens.*, vol. 44, no. 5, pp. 1075–1092, May 2006.
[49] J.P. Magalhães, J.M. N. Vieira, R. Gómez-García, and N.B. Carvalho, "Bio-inspired hybrid filter bank for software-defined radio receivers," *IEEE Trans. Microw. Theory Techn.*, vol. 61, no. 4, pp. 1455–1466, Apr. 2013.
[50] J. Frerick, M. Klumb, R. T. Schieder, V. Tolls, and F. G. Winnewisser, "SWAS-AOS: The first acousto-optical spectrometer in space," *Proc. SPIE*, vol. 3759, pp. 170–179, 1999.
[51] J. T. Johnson et al., "Airborne radio-frequency interference studies at C-band using a digital receiver," *IEEE Trans. Geosci. Remote Sens.*, vol. 44, no. 7, pp. 1974–1985, Jul. 2006.
[52] C. S. Ruf, S.M. Gross, and S. Misra, "RFI detection and mitigation for microwave radiometry with an agile digital detector," *IEEE Trans. Geosci. Remote Sens.*, vol. 44, no. 3, pp. 694–706, Mar. 2006.
[53] J.R. Piepmeier et al., "Radio-frequency interference mitigation for the soil moisture active passive microwave radiometer," *IEEE Trans. Geosci. Remote Sens.*, vol. 52, no. 1, pp. 761–775, Jan. 2014.
[54] J. T. Johnson et al., "Real-time detection and filtering of radio frequency interference onboard a spaceborne microwave radiometer: The CubeRRT mission," *IEEE J. Sel. Topics Appl. Earth Observ. Remote Sens.*, vol. 13, pp. 1610–1624, 2020.
[55] C. Turner, M. Stephen, F. Gambini, G. Chin, P. Racette, and T. Murphy, "Ultra-wideband photonic radiometer for submillimeter wavelength remote sensing," in *Proc. Int. Topical Meeting Microw. Photon.*, 2020, pp. 124–127.
[56] F. Gambini, R. Moreira, A. Gambacorta, J. Klamkin, and M. Stephen, "An innovative photonic integrated channelizer design for hyperspectral microwave sounding," in *Proc. OSA Opt. Sensors Sens. Congr.*, 2021, Art. no. HF4E.5.
[57] Award Information, "Low-power radiation tolerant 4 GHz bandwidth 16k channel spectrometer ASIC," [Online]. Available: https://www.sbir.gov/sbirsearch/detail/1561699
[58] A. Gambacorta et al., "The hyperspectral microwave photonic instrument (HYMPI)," in *Proc. IEEE Int. Geosci. Remote Sens. Symp.*, Kuala Lumpur, Malaysia, 2022, pp. 7206–7209.
[59] A. Gambacorta et al., "The hyperspectral microwave photonic instrument (HYMPI) - advancing our understanding of the Earth's planetary boundary layer from space," in *Proc. IEEE Int. Geosci. Remote Sens. Symp.*, Kuala Lumpur, Malaysia, 2022, pp. 4468–4471.

Antonia Gambacorta received the B.S. degree in physics and the M.S. degree in physics from the Universita' degli Studi A. Moro of Bari, Italy, in 1998 and 2001, respectively, and the M.S. and Ph.D. degrees in atmospheric physics from the University of Maryland Baltimore County, Baltimore, MD, USA, in 2005 and 2008, respectively.

She currently serves a Research Physical Scientist with the Climate and Radiation Laboratory, Goddard Space Flight Center (GSFC), Greenbelt, MD, USA. Prior to joining GSFC, in 2020, she served as the Science Lead of the SNPP, Metop, and JPSS NOAA Unique Combined Atmospheric Processing System (NUCAPS), NOAA/NESDIS/STAR, College Park, MD, USA, and as a Subject Matter Expert in satellite remote sensing for NOAA JPSS. She currently serves as the Principal Investigator of a 2021 NASA Instrument Incubation Project titled: "Photonic Integrated Circuits in Space: The Hyperspectral Microwave Photonic Instrument (HyMPI)" and of a 2021 Decadal Survey Incubation (DSI) Planetary Boundary Layer project titled: "A Combined Passive-Active, Multi-Sensor Approach to Earth's Planetary Boundary Layer (PBL) Sounding." She is also the Principal Investigator of a NOAA Broad Agency Announcement project titled: "Developing the NOAA Next Generation Hyperspectral Microwave Sensor (HyMS): Instrument Concept and Demonstration of Benefits for the NOAA Mission." Her research interests include passive (hyperspectral microwave and Infrared) and active (backscatter lidar) remote sensing techniques and inverse methods for the retrieval of atmospheric temperature and constituents; Earth's planetary boundary layer remote sensing and science applications; and climate feedbacks to greenhouse gas forcing.

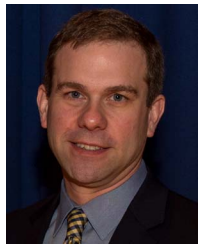

Jeffrey Piepmeier (Fellow, IEEE) received the B.S. engineering degree in electrical concentration from LeTourneau University, Longview, TX, USA, in 1993, and the M.S. and Ph.D. degrees in electrical engineering from Georgia Institute of Technology, Atlanta, GA, USA, in 1994 and 1999, respectively.

He is currently a Chief Engineer for passive microwave instruments with NASA's Goddard Space Flight Center (GSFC), Greenbelt, MD, USA, in the Instrument Systems and Technology Division. He is Deputy Project Manager of Technical for NASA's Atmosphere Observing System and Instrument Scientist for the SMAP microwave radiometer. He is technology Co-Lead of NASA's Planetary Boundary Layer Decadal Survey Incubator Incubation Team for passive sensing. He has co-led multiple mission studies and served as an instrument Subject Matter Expert on the NOAA Satellite Observing System Architecture study. He also contributed to various leadership roles on the cubesat projects IceCube, CubeRRT, and SNOOPI. Previously at GSFC, he was Associate Head, Microwave Instruments and Technology Branch, Instrument Scientist for the GPM Microwave Imager, and Instrument System Engineer for the Aquarius microwave radiometer. Prior to NASA, he worked with Vertex Communications Corporation and was a Shackleford Fellow with the Georgia Tech Research Institute. His research interests include microwave radiometry and technology development to enable the next generation of microwave sensors.

Dr. Piepmeier is a Member of URSI (Commission F). He was the recipient of NASA's Exceptional Engineering Achievement Medal, Exceptional Achievement Medal, and Outstanding Leadership Medal, Department of Commerce's NOAA Bronze Medal, and multiple NASA Group Achievement Awards. He was the past Chairperson of the National Academies' Committee on Radio Frequencies.

Mark Stephen was born in the United States, in 1970. He received the B.S. degree in physics from the University of Delaware, Newark, DE, USA, in 1992, and the M.S. and Ph.D. degrees in applied physics from the University of Maryland Baltimore County, Baltimore, MD, USA, in 2003 and 2008, respectively.

He has worked with NASA's Goddard Space Flight Center, Greenbelt, MD, USA, since 1991, developing laser and electro-optics technologies for space-based applications. He developed diode-pumped solid-state laser systems with an emphasis on laser diode array pumps and the space-qualification of these components, the use of fiber amplifier technology for gas detection and remote sensing using laser spectroscopy and new laser architectures including waveguides. He lead the development of a fiber-based laser transmitter system to measure carbon dioxide in the Earth's atmosphere. He worked on several satellite programs including: the Geoscience Laser Altimeter System, the Mercury Laser Altimeter, and the Lunar Orbiter Laser Altimeter. He was the Product Development Lead for the Advanced Technology Laser Altimeter System Laser, which is currently flying aboard ICESat-2. He is currently working on photonic integrated circuits and mapping lidars for space applications. His research interests include lasers, optical components, and laser instruments.

Joseph Santanello received the M.S. degree in meteorology from Pennsylvania State University, State College, PA, USA, in 1999, and the Ph.D. degree in geography from Boston University, Boston, MA, USA, in 2005.

He leads the GEWEX LoCo working group focused on coordinating international efforts to diagnose and improve land–atmosphere interactions in models from local to global scales, over the last 15 years. He serves as Land Team lead of the NASA Unified WRF (NU-WRF) modeling system, which includes coupling to NASA's Land Information System and facilitates model-data fusion research in the realm of land data assimilation (e.g., soil moisture) and land surface model calibration (e.g., surface fluxes). He currently serves as the Lead of GSFC working group supporting NASA's Decadal Survey Incubation efforts for the PBL, assessing current capabilities and limitations of satellite remote sensing to routinely monitor the PBL for land surface and land–atmosphere studies and modeling, including engagement of GSFC and mission science teams, as well as the PBL community in response to the 2017 Decadal Survey.

John Blaisdell was born in Buffalo, NY, USA, on July 12, 1956. He received the B.A. degree in mathematics and the B.S. degree in physics from the University of Rochester, Rochester, NY, USA, in 1978, and the M.S. and Ph.D. degrees from the University of Illinois, Urbana, IL, USA, in 1978 and 1980, respectively, both in physics.

His dissertation research covered electronic structure of metal oxide semiconductors in the vicinity of surface defects. From 1982 to 1983, he was at the Chemistry Department, Johns Hopkins University, Baltimore, MD, USA, where he studied the electronic structure of molecular crystals. He has been with Science Applications International Corporation/General Sciences Corporation, Beltsville, MD, USA, since 1983, working on space and atmospheric applications. Since 1993, he has been implementing scientific algorithms for atmospheric sounding applications.

Isaac Moradi received the Ph.D. degree in climatology and environmental planning from Kharazmi University of Tehran, Iran, in 2006, and the Ph.D. degree in radio and space science from the Chalmers University of Technology, Gothenburg, Sweden, in 2015.

He is a Research Scientist with the University of Maryland, College Park, MD, USA, affiliated with NASA Global Modelling and Assimilation Office and the NOAA Cooperative Institute for Satellite Earth System Studies, Washington, DC, USA. He is currently the Principal Investigator of several projects focused on advancing the assimilation of all-sky microwave and radar observations into NWP models by improving the forward radiative transfer models and observation error modeling. His research interests include microwave radiative transfer modeling, observing system simulation experiments, satellite data assimilation, calibration of microwave satellite observations, and developing microwave instruments.

William McCarty received the B.S. degree in meteorology from Valparaiso University, Valparaiso, IN, USA, in 2003, and the M.S. and Ph.D. degrees in atmospheric science from the University of Alabama, Huntsville, AL, USA, in 2005 and 2008, under the tutelage of scientists at NASA Marshall Space Flight Center.

He is a Program Scientist in the Weather and Atmospheric Dynamics (WAD) Focus Area. Within this area, he serves as the Program Manager for Weather, Atmospheric Dynamics, and Precipitation Science. He is also the Program Scientist for several instruments that fall within the WAD Focus Area, as well as for the Global Hydrometeorology Resource Center (GHRC) and the Commercial Smallsat Data Acquisition (CSDA) Program. Prior to joining NASA Headquarters, he served as a Research Meteorologist for the Global Modeling and Assimilation Office, NASA Goddard Space Flight Center, Greenbelt, MD, USA, where he focused on satellite data assimilation. He led the Atmospheric Observations group and worked toward the additional and improved use of satellite observations within the GMAO system. His efforts targeted past, present, and future observations through his work on reanalysis, near real-time atmospheric modeling, and data assimilation systems, and observing system simulation experiments. In addition, at Goddard, he served as the first Project Scientist with the CSDA Program, assisting in the on ramp and evaluation of new data vendors. His dissertation focused on the assimilation of Atmospheric Infrared Sounder radiances with the aim of improving short-term numerical weather forecasts. His research interests a broad range of remotely sensed and conventional observations.

Robert Rosenberg received the B.S. degree in Earth and space science and the M.S. degree in mechanical engineering from SUNY Stony Brook, NY, USA, in 1976 and 1977, respectively.

He has 46 years continuous service to NASA projects as a Scientific Programmer/Analyst, Meteorologist, Team Leader, and Program Manager. He currently manages two NASA Earth science projects: the Atmospheric Modeling and Data Assimilation and the NASA Land Information Systems. He has also used his programming and meteorological expertise to support science research initiatives, starting with the First GARP Global Experiment, and recently including the AIRS Sounder Science Team, for which he designed and ran observing system experiments to test the impact of AIRS/AMSU temperature retrievals on forecast skill using the NASA GEOS-5 Data Assimilation and modeling system. He works with the NASA HyMPI team assisting in observing system simulation experiments.

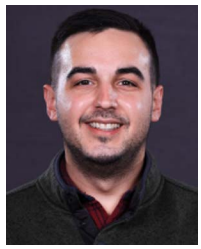

Alexander Kotsakis received the B.S. degree in meteorology with Valparaiso University, Valparaiso, IN, USA, in 2013, and the Ph.D. degree in atmospheric science with the University of Houston, Houston, TX, USA, in 2017.

He is currently an Assistant Research Scientist with ERT, Inc (contractor to NASA GSFC). He has extensive experience utilizing remote sensing measurements and meteorological data together to better understand atmospheric processes. He has extensive experience calibrating, operating, and analyzing balloon borne (radiosonde, ozonesonde) and ground-based remote sensing (Lidars, Pandora–UV-Vis) instrumentation. He has performed research comparing trace gas satellite retrievals (OMI, TROPOMI, etc.) to the ground-based instrumentation. He is currently supporting the development of an AI/ML planetary boundary layer (PBL) retrieval algorithm using his extensive knowledge of the boundary layer meteorology and assists in trade studies for future hyperspectral microwave sensors.

Fabrizio Gambini received the B.S. and M.S. degrees in telecommunication engineering from Politecnico di Milano, Milan, Italy, in 2010 and 2012, respectively, and the Ph.D. degree in emerging digital technologies (curriculum: Photonics Technologies) from Scuola Superiore Sant'Anna, Pisa, Italy, in 2016.

In 2016, he was a visiting Ph.D. student at the Integrated Photonics Laboratory, University of California Santa Barbara (UCSB), Santa Barbara, CA, USA. He was also with the National Inter-University Consortium for Telecommunications, Pisa, as a Research Assistant within the European Project IRIS, developing a high-capacity and reconfigurable wavelength-division multiplexing photonic switch based on ring resonators. In 2018, he joined the Integrated Photonics Laboratory, UCSB, as a Postdoctoral Research Associate working on the design, fabrication, and characterization of photonic integrated devices for data center interconnects, free space communications, and remote sensing for Earth science applications. In 2021, he joined University of Maryland Baltimore County, Baltimore, MD, USA, and the CRESST II program with NASA's Goddard Space Flight Center, Greenbelt, MD, USA, as an Assistant Research Engineer. He is currently developing photonic integrated circuits for hyperspectral remote sensing and lidar applications. His research interests include the study, design, and characterization of photonic integrated devices based on silicon on insulator and indium phosphide technology platforms for datacom and telecommunication applications.

Priscilla Mohammed (Member, IEEE) received the B.S. degree in electrical engineering from the Florida Institute of Technology, Melbourne, FL, USA, in 1999, and the M.S. and Ph.D. degrees in electrical engineering from the Georgia Institute of Technology, Atlanta, GA, USA, in 2001 and 2005, respectively.

She is currently with Goddard Earth Sciences Technology and Research (GESTAR II), Baltimore, MD, USA, as a member of the Morgan State University Research Faculty and also with the Microwave Instrument Technology Branch, NASA's Goddard Space Flight Center, Greenbelt, MD, USA. She is currently a member of the algorithm development team for the soil moisture active passive radiometer. Her research interests include radio frequency interference mitigation in microwave radiometers.

Dr. Mohammed is also a member of the technical committee for Frequency Allocations in Remote Sensing.

Rachael Kroodsma (Member, IEEE) received the B.S.E. degree in Earth systems science and engineering, the M.S.E. degree in electrical engineering, and the Ph.D. degree in atmospheric, oceanic, and space sciences from the University of Michigan, Ann Arbor, MI, USA, in 2009, 2013, and 2014, respectively.

She is currently an Assistant Research Scientist with the Earth System Science Interdisciplinary Center, University of Maryland at College Park, College Park, MD, USA. She is also with the Precipitation Processing System, NASA Goddard Space Flight Center, Greenbelt, MD, USA. Her research interests include microwave radiometer calibration/intercalibration and remote sensing of the atmosphere from airborne and spaceborne sensors.

James MacKinnon received the B.S. and M.S. degrees in computer engineering from the University of Florida, Gainesville, FL, USA, in 2014 and 2016.

He is currently a Computer Engineer with the Science Data Processing branch, NASA Goddard Space Flight Center, Greenbelt, MD, USA. His most recent work includes developing the payload data processing FPGA design for the NASA-developed CeREs CubeSat, and being a Principal investigator on an internal RD project with the goal of designing a neural network for detecting wildfires from multispectral imagery. His expertise includes FPGA design for high-performance, space-based data processing systems, machine learning for science data, and reliable software design.

Ian Adams received the Ph.D. degree in electrical engineering from the University of Central Florida, Orlando, FL, USA, in 2007.

From 2004 to 2006, he was a consultant at Microwave Remote Sensing Consultants, based in Cocoa Beach, FL, USA. From 2006 to 2017, he was employed at the Naval Research Laboratory, Washington, DC, USA, where he studied the effects of precipitation on passive polarimetric remote sensing of ocean surface winds as well as vector radiative transfer of clouds and precipitation. He is currently the Chief Technologist of the Earth Science Division, NASA Goddard Space Flight Centerr, Greenbelt, MD, USA, as well Principal Investigator for the Conical Scanning Millimeter-wave Imaging Radiometer (CoSMIR) and the Configurable Scanning Submillimeter-wave Instrument/Radiometer (CoSSMIR), which recently flew for the first time in over a decade with new polarimetric capabilities. His research interests include microwave remote sensing (particularly at millimeter and submillimeter wavelengths), general remote sensing technology, and the remote sensing of clouds and precipitation.

Dr. Adams is a member of the American Geophysical Union. He served as Vice-Chair of the GRSS Frequency Allocation in Sensing Technical Committee from 2010 to 2013.

Paul Racette received the bachelor's and the master's of science degrees in electrical engineering from the University of Kansas, Lawrence, KS, USA, in 1988 and 1990, respectively, and the doctor of science degree in electrical engineering from George Washington University, Washington, DC, USA, in 2005.

He is a Senior Engineer with the NASA Goddard Space Flight Center, Greenbelt, MD, USA, where he has worked, since 1990. As a member of the Microwave Instruments Technology Branch, he conceives, develops, and deploys remote sensors and sensor technologies for space applications. For the past several years, he has worked to advance digital spectrometry and its application to hyperspectral remote sensing and exploration of the solar system. He is committed to promoting diversity and inclusion in the workplace and serves on Goddard's Native American Employee Resource Group. Beyond his research in digital spectroscopy, he is an Observation Theorist with research interests that include the study and modeling of non stationary processes, calibration methodologies and the role of consciousness in the evolution of the universe.